LETTER

doi:10.1038/nature25508

Global patterns of tropical forest fragmentation

Franziska Taubert[1], Rico Fischer[1], Jürgen Groeneveld[1,2], Sebastian Lehmann[1], Michael S. Müller[1], Edna Rödig[1], Thorsten Wiegand[1,3] & Andreas Huth[1,3,4]

Remote sensing enables the quantification of tropical deforestation with high spatial resolution[1,2]. This in-depth mapping has led to substantial advances in the analysis of continent-wide fragmentation of tropical forests[1–4]. Here we identified approximately 130 million forest fragments in three continents that show surprisingly similar power-law size and perimeter distributions as well as fractal dimensions. Power-law distributions[5–7] have been observed in many natural phenomena[8,9] such as wildfires, landslides and earthquakes. The principles of percolation theory[7,10,11] provide one explanation for the observed patterns, and suggest that forest fragmentation is close to the critical point of percolation; simulation modelling also supports this hypothesis. The observed patterns emerge not only from random deforestation, which can be described by percolation theory[10,11], but also from a wide range of deforestation and forest-recovery regimes. Our models predict that additional forest loss will result in a large increase in the total number of forest fragments—at maximum by a factor of 33 over 50 years—as well as a decrease in their size, and that these consequences could be partly mitigated by reforestation and forest protection.

Tropical forests have a key role in the global carbon cycle[12] and harbour more than half of the known species worldwide[13]. In recent decades, increases in agriculture, logging and urban growth have led to unprecedented losses of tropical forest[14,15], with annual deforestation rates of around 0.5% since the 1990s[1]. Deforestation rates differ between continents[1], with hot spots concentrated mainly in Asia and Brazil[14]. A reduction of forested area is concomitant with fragmentation, in which patches of forest are split into several smaller ones[16]. The increasing availability of high-resolution satellite imagery now enables in-depth mapping of global deforestation[1–4] and detailed analysis of the spatial pattern of the remaining forest.

Here we used percolation theory[10,11] as a framework for analysing the current fragmentation structures in tropical and subtropical regions of the Americas, Africa, and Asia and Australia (denoted here as Asia–Australia) (Fig. 1) on a high-resolution forest cover map[2] (approximately 21 billion pixels, each 30 m × 30 m). We used a clustering algorithm to count and analyse the size and perimeter distribution of all detectable forest fragments separately for each continent, and determined the fractal dimension of the fragmented landscape (Table 1). In total, we identified more than 130 million forest fragments across all continents studied, with sizes ranging over eleven orders of magnitude and reaching 427 Mha. South America's largest forest fragment, in the Amazon, spans around 45% of its total forest area, whereas the largest fragment on Borneo in Asia covers only 18% of the forest.

We expected notably different fragmentation structures between continents owing to different land use practices[14]. However, we observed markedly similar fragment size distributions (Fig. 1), which could be described by power laws[5–7] with almost identical exponents (Table 1). About 10% of continental forest area is made up of forest fragments smaller than 10,000 ha (11.2% for the Americas, 9.9% for Africa and 9.2% for Asia–Australia). Additionally, the fractal dimensions of forest cover are similar for all three continents, with values of approximately 1.9 (Table 1). To analyse the shape of the fragments, we determined the fragment perimeter distributions; again, for all three continents, we found power-law behaviour with similar exponents, with values close to 2.2 (Table 1, Extended Data Fig. 1). Our results raise the

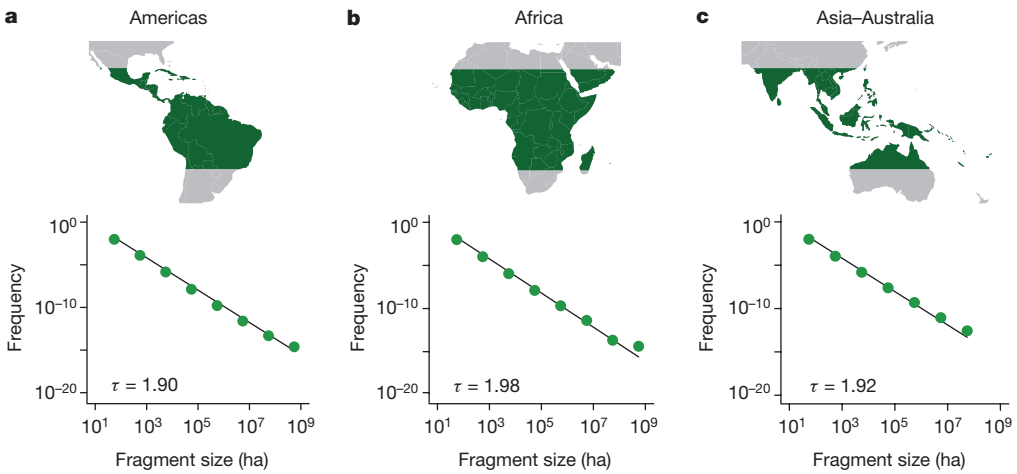

Figure 1 | Continental-scale fragment size distribution of tropical and subtropical forests. a–c, Observed forest fragment size distribution (green dots, fragment sizes ≥10 ha) for the Americas (**a**, $n = 55.5$ million fragments), Africa (**b**, $n = 44.8$ million fragments) and Asia–Australia (**c**, $n = 30.5$ million fragments). The solid lines represent the fits of power-law distributions with exponent τ. The maps show the entire land area of the tropical belt and indicate the selected tropical regions in green. Maps were created using R (ref. 31) and the package 'rworldmap' (ref. 32). Fragment sizes were estimated from Hansen's vegetation cover map[2].

[1]Helmholtz Centre for Environmental Research – UFZ, Department of Ecological Modelling, Permoserstrasse 15, 04318 Leipzig, Germany. [2]TU Dresden, Institute of Forest Growth and Forest Computer Sciences, PO 1117, 01735 Tharandt, Germany. [3]German Centre for Integrative Biodiversity Research (iDiv) Halle-Jena-Leipzig, Deutscher Platz 5e, 04103 Leipzig, Germany. [4]University of Osnabrück, Institute of Environmental Systems Research, Barbarastrasse 12, 49076 Osnabrück, Germany.

Table 1 | Continental-scale fragmentation of tropical forests

	Americas	Africa	Asia–Australia	Theory*
Forest area in Mha	940	577	391	
Number of fragments (n)	55,558,018	44,851,251	30,556,204	
Mean (median) size of fragments in ha	17 (0.09)	13 (0.09)	13 (0.09)	
Forest area (%) of fragments <10,000 ha	11.2	9.9	9.2	
Fragment size scaling†,‡ (τ)	1.90	1.98	1.92	2.05
Fractal dimension§ (d_f)	1.92	1.87	1.87	1.89
Perimeter scaling†,‖ (κ)	2.16	2.23	2.21	2.14

All features were calculated on the basis of a high-resolution forest cover map[2]. Annual gross deforestation rates[1] of 0.51% (Americas), 0.37% (Africa) and 0.62% (Asia–Australia) for the years 2000–2010.
*Theoretical values according to percolation theory[10,11] (near the critical point).
†The term 'scaling' refers to the exponent of the fitted power-law distributions. The calculation of fragment size and perimeter scaling is based on $n = 55.5$ million (Americas), $n = 44.8$ million (Africa) and $n = 30.5$ million (Asia–Australia) fragments. See Methods for details.
‡Pearson's correlation coefficients (R) and standard errors (ε) are: $R^2 = 0.96$ and $\varepsilon = 0.0011$ (Americas), $R^2 = 0.956$ and $\varepsilon = 0.0017$ (Africa), $R^2 = 0.958$ and $\varepsilon = 0.0022$ (Asia–Australia). Deviations from the theoretical expectation trace back to the finite area of the continents.
§The fractal dimension is based on the analysis of $n = 8$ different grid sizes, see Methods for details. The estimate of the fractal dimension is not affected by landscape area.
‖Pearson's correlation coefficients (R) and standard errors (ε) are: $R^2 = 0.952$ and $\varepsilon = 0.00082$ (Americas), $R^2 = 0.931$ and $\varepsilon = 0.0011$ (Africa), $R^2 = 0.938$ and $\varepsilon = 0.0015$ (Asia–Australia).

question of why varying patterns of local deforestation produce fragmentation patterns that are so similar at the continental scale.

Percolation theory[10,11] provides one possible explanation for the observed patterns. In this theory, the probability that the cells of a landscape are occupied by forest is designated p. Where occupied cells share at least one side with another, a forest fragment (also known as a cluster) is formed. If p is large, the landscape is dominated by one large fragment spanning the whole area (Extended Data Fig. 2a). For lower values of p the forest landscape is divided into smaller fragments, although there is still one large fragment (known as the spanning cluster) that connects one side of the landscape with the other. It should be noted that the spanning cluster can form complex shapes with larger holes[11] (Extended Data Fig. 2b). When the probability p falls to a certain level (approximately that of the critical point, $p_c = 0.59$, which indicates 59% forest area for large landscapes), the spanning cluster breaks up and smaller fragments appear (Extended Data Fig. 2c, d).

The phases of fragmentation below and above a forest cover of 59% are defined as subcritical and supercritical, respectively, whereas the value of $p_c = 0.59$ itself represents the critical point of percolation at which the large-scale behaviour of the system can be described by simple mathematical relationships[11,17]. For example, percolation theory predicts that the size distribution of fragments can be described by a power law with an exponent τ of approximately 2.05 at the critical point (for infinite landscapes[10,11]). Notably, the empirical exponents of the forest cover map agree with the theory, with τ values of between 1.9 and 2.0 (Table 1). At the critical point, the exponent of the fragment size distribution τ is further related to the fractal dimension d_f via the hyperscaling relationship[11,18,19] $\tau = 1 + 2/d_f$. Theory predicts a fractal dimension of 1.89 at the critical point[11], which is in agreement with the d_f values determined for the high-resolution forest cover map (1.92 for the Americas and 1.87 for Africa and Asia–Australia, Table 1). The obtained perimeter distributions (Table 1) also show power laws in agreement with the theoretical exponent[20] κ of approximately 2.14. Such critical exponents are often fingerprints of the hidden dynamics of a system[7,9,21].

Our empirical findings suggest that the observed tropical forest fragmentation is near to the critical point of percolation in all three continents (reference year 2000). To test this hypothesis and to explore future dynamics, we developed and analysed three dynamic fragmentation models: FRAG, FRAG-B and FRAG-P. In the FRAG model, which corresponds to classical percolation theory[11], local forest sites are cleared randomly and independently each year[22,23] (Fig. 2, Extended Data Fig. 3, Supplementary Video 1). Deforestation occurs across a landscape initially covered by forest. The FRAG-B and FRAG-P models were used to test our findings with respect to more complex deforestation and reforestation patterns as well as forest protection (see Methods for details). We analysed the dynamics of forest fragmentation for each continent and monitored all forest fragments emerging over time. In total, approximately 3 Gha of forest area was simulated (33 billion cells of resolution 30 m × 30 m).

The dynamics of forest fragmentation as simulated by the FRAG model predict the empirically observed fragment size distributions (Fig. 2b). For forest removal beyond the critical point, the development of the number of fragments shows a 'hump-shaped' behaviour[24] (Fig. 3a, b). The number of fragments increases slowly before the critical point, but accelerates sharply afterwards (to a maximum of 2,000 million fragments for the tropical Americas, Fig. 3a). The number of fragments currently observed and their mean size also match the predictions of the FRAG model close to the critical point (Fig. 3a, b). Small additional amounts of forest loss in the near future would lead to a strong

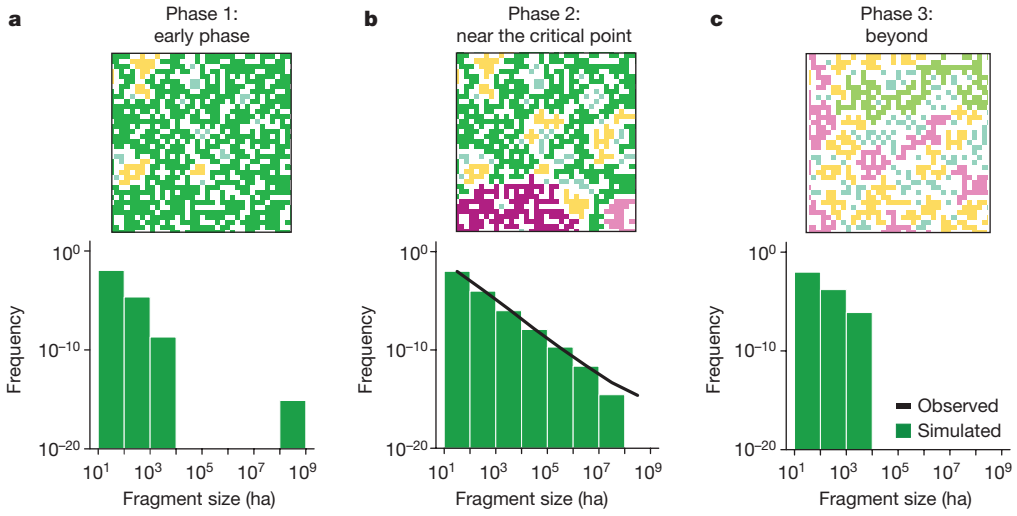

Figure 2 | Dynamics of tropical forest fragmentation in the Americas. **a**–**c**, Fragment size distributions (green bars, FRAG simulation; black line, observations from remote sensing; fragment sizes ≥10 ha) and spatial patterns of fragments at different time points: the early phase (**a**), near to the critical point of percolation (**b**) and beyond (**c**). For each phase, a map of a selected subarea of 225 ha is shown (inset, according to the FRAG model); cleared sites are white and the different colours indicate different fragment sizes. Snapshots and a video are provided in Extended Data Fig. 3 and Supplementary Video 1, respectively.

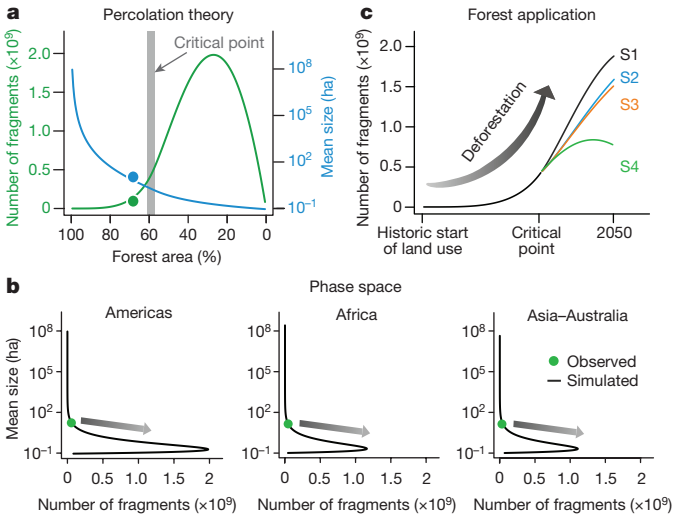

Figure 3 | Percolation theory applied to the observed forest fragmentation. a, Dynamics of the number of forest fragments (green line, linear scale) and mean fragment size (blue line, linear scale) with decreasing forest area, as observed by remote sensing (dots) and simulated by the fragmentation model FRAG (solid lines) for the Americas. **b**, The number of fragments and their mean size show non-linear behaviour for all three continents (solid lines, FRAG simulations; dots, observations from remote sensing). **c**, Application of percolation theory to predict future forest fragmentation for different scenarios in the Americas using the FRAG model (see Methods for details of scenarios S1–S4).

increase in the number of forest fragments. We obtained similar trends for Africa and Asia–Australia (Fig. 3b).

We used the FRAG model to investigate how forest fragmentation would proceed in the coming decades on the basis of our suggested explanation for the observed fragmentation patterns. Under constant deforestation (at a rate of 0.51% per year in the Americas[1] without any reforestation), the number of forest fragments will greatly increase (at maximum by a factor of 33 over 50 years, scenario S1 in Fig. 3c, Extended Data Fig. 4a, e) while the mean sizes of fragments will decrease from 17 ha to 0.25 ha. To assess how reduced deforestation and reforestation may mitigate these effects, we analysed additional scenarios (Fig. 3c, Extended Data Fig. 4b–e). For example, when considering reforestation (at a rate of 0.14% per year in the Americas[1]), the deforestation rate is reduced only slightly and still leads to an increase in the number of fragments, by a factor of 28 until 2050 (scenario S2 in Fig. 3c). The same would result for a yearly reduction in deforestation rate (derived from ref. 2), for which the projected increase in fragment number is limited to a factor of 27 until 2050 (scenario S3 in Fig. 3c). Only efforts that increasingly reduce deforestation rates in combination with reforestation (for example, by 0.01% year^{-2}) would lead to increasing forest cover and decreasing fragment numbers after 20 to 30 years (scenario S4 in Fig. 3c). Such mitigation scenarios are important aspects for an assessment of forest fragmentation. Although Europe, North America and parts of Asia have experienced higher levels of reforestation than deforestation during the past few centuries[25,26], forest loss still exceeds forest gain in most tropical countries[2,26] such as Brazil, Indonesia and Cameroon.

Increases in fragment number and decreases in fragment size both have important consequences for the habitats of species[3,27,28] and for forest fragment edges[16,27]. Negative effects on biodiversity[16,27] arise from a reduction in the connectivity of fragments and the enhancement of edge effects. In addition, recent studies have outlined that increased tree mortality[16] in the edge area of forest fragments will lead to additional carbon emissions[29]. Effective policies and regulations for preventing the negative effects of fragmentation therefore require robust indicators. The development of indicators is an important challenge in environmental science, especially given the possibility that critical transitions of global ecosystems may occur as a result of human land transformations[30].

To test our results with respect to more complex spatial regimes of deforestation (the FRAG-B model), we simulated deforestation to occur with probability d_{border} at the border of already existing forest fragments and at random locations otherwise (Extended Data Fig. 5, Supplementary Video 2). In terms of criticality, the FRAG-B model showed behaviour similar to that of the classical percolation model (FRAG), for nearly the entire range of the parameter d_{border} (critical point at $p_c = 0.59$ with $\tau \sim 2$, Extended Data Fig. 6). In addition, border deforestation further widens the range of forest area in which power-law behaviour with an exponent of $\tau \sim 2$ occurs (Extended Data Fig. 7). Reforestation (for example, 0.14% per year in the Americas[1]) is already well addressed by our FRAG and FRAG-B models by lowering deforestation rates (Extended Data Fig. 8). Similarly, protection of forest (FRAG-P model) proportionally reduces the forest area that is prone to deforestation where the FRAG model still applies (simulated number of fragments scale with landscape size, Extended Data Figs 9, 10). Although local landscape structures may differ owing to local deforestation regimes, we found that the behaviour of the extended models collapses after suitable transformation in good approximation to that of the classical percolation model (FRAG). Reforestation and protecting large forest areas nevertheless have potential to mitigate the consequences of fragmentation (Extended Data Figs 4, 10).

The findings of the extended percolation models underpin the universality of fragmentation patterns close to the critical point. This is a general feature of critical phenomena: their large-scale behaviour is independent of the underlying small-scale mechanisms[7,17,21]. Even though land use appears to be complex and diverse, our outcomes emphasize that simple mechanisms are sufficient for describing forest fragmentation structures at larger scales. This finding does not exclude the possibility that the empirical patterns detected here may have alternative explanations. Our combination of spatial analyses of a high-resolution forest cover map, simulation modelling and the application of percolation theory provides a first step towards a simple explanation for the intriguing global patterns of tropical forest fragmentation.

Online Content Methods, along with any additional Extended Data display items and Source Data, are available in the online version of the paper; references unique to these sections appear only in the online paper.

Received 24 February 2017; accepted 9 January 2018.
Published online 14 February 2018.

1. Achard, F. *et al.* Determination of tropical deforestation rates and related carbon losses from 1990 to 2010. *Glob. Change Biol.* **20,** 2540–2554 (2014).
2. Hansen, M. C. *et al.* High-resolution global maps of 21st-century forest cover change. *Science* **342,** 850–853 (2013).
3. Haddad, N. M. *et al.* Habitat fragmentation and its lasting impact on Earth's ecosystems. *Sci. Adv.* **1,** e1500052 (2015).
4. Chaplin-Kramer, R. *et al.* Degradation in carbon stocks near tropical forest edges. *Nat. Commun.* **6,** 10158 (2015).
5. Storch, D., Marquet, P. A. & Brown, J. H. *Scaling Biodiversity* (Cambridge Univ. Press, 2007).
6. Marquet, P. A. *et al.* Scaling and power-laws in ecological systems. *J. Exp. Biol.* **208,** 1749–1769 (2005).
7. Sornette, D. *Critical Phenomena in Natural Sciences. Chaos, Fractals, Selforganization and Disorder: Concepts and Tools* (Springer, 2006).
8. Turcotte, D. L. & Malamud, B. D. Landslides, forest fires, and earthquakes: examples of self-organized critical behavior. *Physica A* **340,** 580–589 (2004).
9. Bak, P. *How Nature Works. The Science of Self-Organized Criticality* (Copernicus, 1996).
10. Stauffer, D. & Aharony, A. *Introduction to Percolation Theory* (Taylor & Francis, 1994).
11. Christensen, K. & Moloney, N. R. *Complexity and Criticality* Vol. 1 (Imperial College Press, 2005).
12. Le Quéré, C. *et al.* Global carbon budget 2014. *Earth Syst. Sci. Data* **7,** 47–85 (2015).
13. Wright, S. J. Tropical forests in a changing environment. *Trends Ecol. Evol.* **20,** 553–560 (2005).
14. Lewis, S. L., Edwards, D. P. & Galbraith, D. Increasing human dominance of tropical forests. *Science* **349,** 827–832 (2015).
15. Houghton, R. A. The worldwide extent of land-use change. *Bioscience* **44,** 305–313 (1994).

16. Laurance, W. F. *et al.* The fate of Amazonian forest fragments: a 32-year investigation. *Biol. Conserv.* **144,** 56–67 (2011).
17. Saberi, A. A. Recent advances in percolation theory and its applications. *Phys. Rep.* **578,** 1–32 (2015).
18. Milne, B. T. *et al.* Detection of critical densities associated with piñon-juniper woodland ecotones. *Ecology* **77,** 805–821 (1996).
19. Drossel, B. & Schwabl, F. Self-organized critical forest-fire model. *Phys. Rev. Lett.* **69,** 1629–1632 (1992).
20. Ziff, R. M. Test of scaling exponents for percolation-cluster perimeters. *Phys. Rev. Lett.* **56,** 545–548 (1986).
21. Solé, R. V. & Bascompte, J. *Self-Organization in Complex Ecosystems* Vol. 42 (Princeton Univ. Press, 2006).
22. Turner, M. G., Gardner, R. H. & O'Neill, R. V. *Landscape Ecology in Theory and Practice* (Springer, 2001).
23. Gardner, R. H., Milne, B. T., Turner, M. G. & O'Neill, R. V. Neutral models for the analysis of broadscale landscape pattern. *Landsc. Ecol.* **1,** 19–28 (1987).
24. Bascompte, J. & Solé, R. V. Habitat fragmentation and extinction thresholds in spatially explicit models. *J. Anim. Ecol.* **65,** 465–473 (1996).
25. Meyfroidt, P. & Lambin, E. F. Global forest transition: prospects for an end to deforestation. *Annu. Rev. Environ. Resour.* **36,** 343–371 (2011).
26. Rudel, T. K. *et al.* Forest transitions: towards a global understanding of land use change. *Glob. Environ. Change* **15,** 23–31 (2005).
27. Debinski, D. M. & Holt, R. D. A survey and overview of habitat fragmentation experiments. *Conserv. Biol.* **14,** 342–355 (2000).
28. Andrén, H. Effects of habitat fragmentation on birds and mammals in landscapes with different proportions of suitable habitat: a review. *Oikos* **71,** 355–366 (1994).
29. Brinck, K. *et al.* High resolution analysis of tropical forest fragmentation and its impact on the global carbon cycle. *Nat. Commun.* **8,** 14855 (2017).
30. Barnosky, A. D. *et al.* Approaching a state shift in Earth's biosphere. *Nature* **486,** 52–58 (2012).
31. R Core Team. *R: A Language and Environment for Statistical Computing*; https://www.R-project.org/ (R Foundation for Statistical Computing, 2015).
32. South, A. rworldmap: A new R package for mapping global data. *R J.* **3,** 35–43 (2011).

Supplementary Information is available in the online version of the paper.

Acknowledgements The project has been supported by the Helmholtz Alliance Remote Sensing and Earth System Dynamics. A.H. and T.W. were supported by the European Research Council Advanced Grant 233066. We thank A. Hein and A. Bogdanowski for assistance, A. Hartmann for discussion, M. Dantas de Paula for data handling, and S. Paulick and F. Bohn for technical support.

Author Contributions A.H., F.T. and R.F. conceived the project. A.H., F.T. and T.W. supervised the research. S.L. and E.R. processed and analysed vegetation maps. F.T. performed statistical analysis of map observations. F.T. and M.S.M. implemented the simulation models and conducted the simulations. F.T. analysed the results and prepared figures, tables and videos. A.H., F.T., R.F., T.W. and J.G. wrote the manuscript. All authors have participated in discussion and editing of the manuscript.

Author Information Reprints and permissions information is available at www.nature.com/reprints. The authors declare no competing financial interests. Readers are welcome to comment on the online version of the paper. Publisher's note: Springer Nature remains neutral with regard to jurisdictional claims in published maps and institutional affiliations. Correspondence and requests for materials should be addressed to F.T. (franziska.taubert@ufz.de).

Reviewer Information *Nature* thanks B. Barzel, B. DeVries, R. Ewers and P. Marquet for their contribution to the peer review of this work.

METHODS

Use and analysis of the forest cover map. The analysis of global forest fragmentation is based on Hansen's forest cover map[2] that uses Landsat observation for the year 2000 with a spatial resolution of 30 m × 30 m. A forest/non-forest classification threshold of 30% (minimum forest cover per pixel) was used in this study.

The resulting image shows non-forested and forested pixels (the original binary image files were processed as in ref. 29, ASCII format, WGS-84 projection); their connection to forest fragments is determined by their four-pixel neighbourhood (open boundary conditions). For this, an extended cluster detection algorithm was used[29]. The area of a pixel in the WGS-84 projection is calculated dependent on its geographical position[29]. As area calculation for every pixel is highly time-consuming (55 billion pixels for land surface in the tropics), we pre-calculated the area size of pixels along 256 latitudes. No statistical methods were used to predetermine sample size.

Forest fragmentation model FRAG. For simulation of fragmentation dynamics we used a landscape with C_{max} cells of size s (30 m × 30 m). Cells can have two states (forested or deforested). We start the simulation with a fully forested area (all cells are in the 'forest' state, total forest area is A_{max} (landscape area), $A_{max} = C_{max}\, s$). In each step (here, one year) some forest area is cleared assuming a constant deforestation rate d (% per year). That is, a certain number of forest cells ($C_{max}\, d$) are randomly selected and assigned to the state 'deforested' in each year.

For simplicity, cells do not regenerate back to forest in the FRAG model, so forest area is successively reduced over time until the entire forest area is cleared. However, deforestation rates used in the FRAG model can also be interpreted as net deforestation rates that result from reforestation and gross deforestation occurring at random sites. In detail, with d being the yearly gross deforestation rate (for example, 0.51% per year derived from ref. 1 for the tropical Americas) and r being the yearly reforestation rate (for example, 0.14% per year derived from ref. 1 for the tropical Americas), we obtained a yearly net deforestation rate of $d_{net} = d - r$. Including random reforestation into our simulations therefore shows that the effect of reforestation is already covered by the FRAG model (Extended Data Fig. 8a). If reforestation occurs exclusively at the border of forest fragments, small deviations can be observed (median deviations show 5% lower fragment numbers than for random reforestation).

We analysed the results of the fragmentation model using the same methods as for the analysis of the high-resolution forest cover map in terms of remaining forest area, fragment numbers and their mean size as well as the fragment size distribution (see 'Analysis and statistics of tropical forest fragmentation'). Dynamics of fragment numbers scale with landscape size C_{max} (total number of cells, Extended Data Fig. 9a). Normalized fragment numbers can therefore be calculated by dividing the absolute number of fragments by the total number of cells (C_{max}).

The critical point p_c is determined as the remaining forest area relative to landscape area A_{max} after which the spanning cluster no longer exists. The spanning cluster is defined as any large cluster that expands from one border of the landscape to an opposite side border (either north to south or east to west). Note that this simple fragmentation model corresponds to a dynamic version of the classical percolation model[10,11,22,23].

Simulation of forest fragmentation at the continental scale. Potential forest areas before forest clearing have been estimated for each continent using a map of vegetation biomes[33] selecting for classified tropical forest area (only biomes of tropical and subtropical woodland). Potential areas have been calculated by remapping vegetation cover of gridded maps (0.5° × 0.5°) to an equidistant map (1 km × 1 km) using climate data operators[34].

We simulated forest fragmentation dynamics by using, for each continent, the estimated potential forest cover (cell size s = 30 m × 30 m) and deforestation rates derived from literature (Table 1). Extents of simulated continental areas for the fragmentation model were 1,377 million ha for the Americas, 806 million ha for Africa and 770 million ha for Asia–Australia (corresponding to C_{max} values of 15,300,205,636 cells for the Americas, 8,955,593,956 cells for Africa and 8,555,695,009 cells for Asia–Australia). To determine the current forest area (in %) in Fig. 3a, we divided the observed forest areas (from remote sensing, Table 1) by the estimated potential forest areas. Gross deforestation rates (Table 1) and reforestation rates were derived from ref. 1 by dividing area change estimates of annual gross deforestation (2000–2010) and annual forest regrowth (2000–2010) by area estimates of forest cover (2000) for dry and humid tropical forests. It should be noted that potential forest area estimates can include uncertainties that can affect the determined fraction of current forest area (in %) for the forest cover map.

Simulation scenarios of future forest fragmentation patterns. We simulated four different scenarios (S1 to S4) to project future development of forest fragmentation (until 2050 for the Americas, using the FRAG model, Extended Data Fig. 4):

Scenario S1: Net deforestation rate is constant at d_{net} = 0.51% per year (ref. 1). This scenario assumes no reforestation.

Scenario S2: Deforestation of d = 0.51% per year (ref. 1) is counterbalanced by reforestation of r = 0.14% per year (ref. 1). This results in a net deforestation rate of d_{net} = 0.37% per year.

Scenario S3: Deforestation rate of 0.37% per year (ref. 1) is reduced by 0.0012% year^{-2}. This results in a net deforestation rate of $d_{net} = a - bt$, with t being the number of years since the critical point, a = 0.37% per year and b = 0.0012% year^{-2}. This scenario for the tropical Americas was based on a 12-year observation of forest gain and forest loss (ref. 2, version v1.3). The derived absolute values of net forest area change were related to our simulated landscape area (A_{max}) and fitted by linear regression (slope = 0.0012, R^2 = 0.013).

Scenario S4: Deforestation of 0.37% per year (ref. 1) is reduced by 0.01% year^{-2}. This results in a net deforestation rate of $d_{net} = a - bt$ (with a = 0.37% per year and b = 0.01% year^{-2}) with a turning point at which forest recovery exceeds deforestation. This scenario is similar to S3, but with a stronger decreasing trend of yearly deforestation rates.

Projections of future fragmentation for the year 2050 started from the critical point of percolation using the FRAG model (as a simplification). A time step corresponds to a constant reduction of forest area per year. Projected values (of fragment numbers and mean size in 2050) for different deforestation scenarios (Fig. 3c) were compared to observational values from remote sensing (Table 1, factors shown in Extended Data Fig. 4). The fragmentation dynamics (in terms of deforestation rate, forest cover, fragment numbers and mean fragment size) for each scenario are shown in Extended Data Fig. 4 (absolute values can be found in Extended Data Fig. 4e).

Forest fragmentation model FRAG-B. In addition, we analysed a second version of the fragmentation model in order to test for more complex deforestation patterns. Here, a probability d_{border} of clearing only forested cells at the border of a forest fragment has been introduced. When d_{border} = 0, forested cells are cleared randomly (FRAG model version). When d_{border} = 0.5, 50% of the deforestation is restricted to fragment borders while the remaining 50% is still deforested randomly throughout the area. When d_{border} = 1, only cells at the border of forest fragments are cleared (with random site selection for deforestation in the first time step). We analysed the result of the FRAG-B model similar to that of the FRAG model (see 'Analysis and statistics of tropical forest fragmentation'). Dynamics of fragment number also scale with landscape size C_{max} (Extended Data Fig. 9b). As such, normalized fragment numbers can again be calculated by dividing the absolute number of fragments by the total number of cells (C_{max}).

Gross deforestation rates used in the FRAG-B model can again be interpreted as net deforestation rates that result from reforestation at random sites together with border gross deforestation (similar to the FRAG model, Extended Data Fig. 8b). In this case, the probability that deforestation occurs at the border of forest fragments (d_{border}) becomes approximately $d_{border,net} = (d_{border}\, d - r)/(d - r)$, with d being the yearly gross deforestation rate (for example, 0.51% per year in the Americas[1]) and r being the yearly reforestation rate (for example, 0.14% per year in the Americas[1]). Small deviations can be attributed to the dynamic change of border area of fragments during the simulation. By contrast, reforestation is fully captured by our FRAG-B model if reforestation occurs with the same probability d_{border} at the border of forest fragments as does deforestation.

In order to test for a full range of border deforestation, we simulated a forest landscape ($C_{max} = 10^6$ cells) and varied d_{border} from 0 to 1 in steps of 0.1. Between d_{border} = 0.9 and d_{border} = 1.0 we tested model behaviour for detailed values: d_{border} = 0.925, 0.95, 0.975, 0.98, 0.985, 0.99, and 0.995 (because critical points and power-law exponents of fragment sizes drop between d_{border} = 0.9 and d_{border} = 1.0). We focused our analysis on the critical points and the fitted power-law exponents of fragment size distributions for each simulation (Extended Data Fig. 6) with the following sample sizes of fragments: n = 29,788 (d_{border} = 0), n = 30,195 (d_{border} = 0.1), n = 29,020 (d_{border} = 0.2), n = 28,131 (d_{border} = 0.3), n = 31,117 (d_{border} = 0.4), n = 30,506 (d_{border} = 0.5), n = 30,733 (d_{border} = 0.6), n = 34,182 (d_{border} = 0.7), n = 35,325 (d_{border} = 0.8), n = 43,045 (d_{border} = 0.9), n = 44,997 (d_{border} = 0.925), n = 45,964 (d_{border} = 0.95), n = 45,577 (d_{border} = 0.975), n = 44,415 (d_{border} = 0.98), n = 45,692 (d_{border} = 0.985), n = 43,806 (d_{border} = 0.99), n = 38,875 (d_{border} = 0.995), n = 1,278 (d_{border} = 1.0).

Forest fragmentation model FRAG-P. A third version of the fragmentation model includes protected forest areas. Here, a fraction $f_{protected}$ of landscape area (in total $f_{protected}\, A_{max}$) is preserved against deforestation. When $f_{protected}$ = 0, forest area is cleared randomly (FRAG model). When $f_{protected}$ = 0.5, 50% of forest area is protected while the remaining 50% is still deforested randomly. When $f_{protected}$ = 1, no forest area is cleared. The protected forest area is distributed among rectangular forest patches (10,000 ha in size) that are randomly distributed across the landscape. In order to reach the total protected area exactly ($f_{protected}\, A_{max}$), a few forest patches of different sizes are also assigned for protection (for example, if protected forest patches overlap or are placed too close to the landscape boundaries).

Conceptually, protecting large forest fragments means preserving certain size classes in the fragment size distribution (for example, in our FRAG-P model the sizes from 10^4 ha to 10^5 ha). Therefore, protection of one large fragment is equivalent to excluding this fragment from the study area prone to deforestation (for example, similar to the FRAG model). Because the normalized number of fragments (normalization means dividing by the total number of cells C_{max}) is independent of landscape size, we obtain a behaviour that is captured by the FRAG model for smaller landscape areas as well (Extended Data Fig. 9). This property reduces the extrapolated number of forest fragments proportionally by $(1 - f_{protected})$ (Extended Data Fig. 10).

In order to test for a range of protected forest area, we simulated different fractions of protected areas ($f_{protected} = 0.1$ and 0.5, for landscape sizes compared to the tropical Americas; that is, $C_{max} = 15{,}300{,}205{,}636$ cells). We focused our analysis on the number of forest fragments (Extended Data Fig. 10).

Analysis and statistics of tropical forest fragmentation. Forest fragments were detected by applying an extended cluster detection algorithm[29]. This algorithm labels each single fragment of cells on the basis of the direct four neighbours per cell (see 'Use and analysis of the forest cover map'). The mean fragment size of a landscape is calculated by summing up their sizes divided by the number of fragments (unweighted mean including the spanning cluster).

We calculated the fragment size distribution, that is the number of fragments per fragment size class. In order to describe its form, we applied multinomial maximum likelihood estimation of logarithmically binned data to fragment sizes published in ref. 35 (using the MATLAB package provided online). We fitted the frequency of fragment sizes to a power-law distribution to determine the scaling exponent ($N(f) \sim f^{-\tau}$, where $N(f)$ is the number of fragments of size f and τ is the scaling exponent). For logarithmic binning, we used size classes (in ha) of $[10^1, 10^2)$, $[10^2, 10^3)$, … $[10^8, 10^9)$. We excluded fragments smaller than 10 ha for the fit. Standard errors[35] for each fitted exponent were calculated by bootstrapping (1,000 repetitions). Goodness of fit was evaluated by using Pearson's correlation coefficient (R) between predicted and empirical cumulative distributions (both logarithmic; using raw data including also empirical and simulated fragments smaller than 10 ha). Similar to fragment sizes, we calculated perimeters (edge length) of detected forest fragments for analysing and fitting the fragment perimeter distribution ($N(l) \sim l^{-\kappa}$, where $N(l)$ is the frequency of fragments with perimeter l and κ is the scaling exponent). For logarithmic binning, we used perimeter classes $[10^3, 10^4)$, $[10^4, 10^5)$, … $[10^9, 10^{10})$ in m and excluded fragment perimeters smaller than 1,000 m for the fit (equivalent to a fragment size of approximately 10 ha). Standard errors[35] were again derived for each fitted exponent by bootstrapping (1,000 repetitions). Goodness of fit was similarly evaluated by using Pearson's correlation coefficient (R) between predicted and empirical cumulative distributions (both logarithmic; using raw data including also empirical and simulated fragment perimeters smaller than 1,000 m).

We further determined the fractal dimension d_f on the basis of subsequently grouping 30 m × 30 m cells of the vegetation map to boxes of $b_f = 2^1, 2^2, 2^3, \ldots, 2^8$ cells (box counting method[36,37]). For each box, we determined how many cells include forest. When at least one cell per box is occupied by forest, we mark the entire box as forested. By this method, a map is created that has coarser resolution than the original map (with $s = 30\,m \times 30\,m$ resolution). The fractal dimension is then calculated by relating the inverse of b_f to the number of boxes including forest on the landscape of coarser resolution. This relationship follows a power law, the scaling exponent of which represents the fractal dimension. We fitted this relationship on log–log axes by using ordinary least squares regression and calculated the corresponding coefficient of determination R^2. We calculated the fractal dimension d_f for the high-resolution vegetation map (Table 1, with R^2 values of approximately 1 for each continent) and compared them to the predicted dimension $d_f = 1.89$ of percolation theory[11]. It should be noted that deviations in the exponent τ of the fragment size distribution trace back to the finite area of the continents, whereas the calculation of fractal dimension is not affected by the finite area.

The large extent of our simulated forest landscapes shows low variations in results for ten replicated simulations. We calculated the coefficient of variation CV (standard deviation σ divided by mean value μ, $CV = \sigma/\mu$) from ten repeated simulations for each time step. Finally, we determined the median value, CV_{median}, as an aggregated statistic for all time steps for the number and mean size of fragments. For the fragment size distribution, we calculated the CV only at the critical point for each class of fragment sizes and determined the median CV_{median} for all size classes (details of size classes are provided earlier in this section). For fragment number and mean size, median CV_{median} values were below 0.00004 for all three continents (using the FRAG model, CV_{median} decreased in general during the simulation time). Median CV_{median} among size classes of the fragment size distribution (at the critical point) were less than 0.0062 (CV_{median} decreased in general with smaller size classes). Similar results were obtained for the FRAG-B (0.00004 and 0.0036 for $d_{border} = 0.9$, landscape area of the Americas) and FRAG-P models (0.00003 and 0.448 for $f_{protected} = 0.1$, landscape area of the Americas). Because stochasticity did not translate into visible effects, we visualized only one simulation run in Fig. 2, Fig. 3 and Extended Data Figs 3–10 and provided absolute values of one simulation run in Extended Data Fig. 4e.

Visualization of fragmentation patterns. We gathered snapshots of fragment size distributions and spatial patterns for each simulated year in our FRAG and FRAG-B models for the Americas, as MPG files (Supplementary Videos 1, 2) and figures (Fig. 2, Extended Data Figs 3, 5). For the fragment size distribution, green bars show the simulation results (FRAG or FRAG-B models) and the black line shows the observed size distribution (from remote sensing) for the tropical forest in the Americas. We used logarithmic binning of fragment size classes $[10^1, 10^2)$, $[10^2, 10^3)$, … $[10^9, 10^{10})$ in ha. For graphical purposes only, we additionally visualized size classes $[10^{-1}, 10^0)$ and $[10^0, 10^1)$. The remaining forest area (p) is provided within the bar plot of the videos. For the map shown (a selected subarea of 900 ha was used for Extended Data Figs 3 and 5 as well as for Supplementary Videos 1 and 2; a selected subarea of 225 ha was used for Fig. 2 for graphical purposes), each fragment is coloured according to its size. Six size classes (x, in ha) were chosen with the following colour codes: $x < 0.4$ (light blue), $0.4 \le x < 2$ (yellow), $2 \le x < 9$ (light magenta), $9 \le x < 42$ (light green), $42 \le x < 195$ (dark magenta), $x \ge 195$ (dark green). White cells denote cleared sites.

Code availability. The extended cluster detection software and the simulation models are available upon request from the corresponding author.

Data availability. The observed fragment-size and perimeter-distribution data, as well as the data of the simulation studies, are available upon request from the corresponding author.

33. Ostberg, S., Schaphoff, S., Lucht, W. & Gerten, D. Three centuries of dual pressure from land use and climate change on the biosphere. *Environ. Res. Lett.* **10,** 044011 (2015).
34. CDO 2015: Climate Data Operators. *The Max Planck Institute for Meteorology*, http://www.mpimet.mpg.de/cdo (2017).
35. Virkar, Y. & Clauset, A. Power-law distributions in binned empirical data. *Ann. Appl. Stat.* **8,** 89–119 (2014).
36. Sugihara, G. & May, R. M. Applications of fractals in ecology. *Trends Ecol. Evol.* **5,** 79–86 (1990).
37. Bisoi, A. K. & Mishra, J. On calculation of fractal dimension of images. *Pattern Recognit. Lett.* **22,** 631–637 (2001).

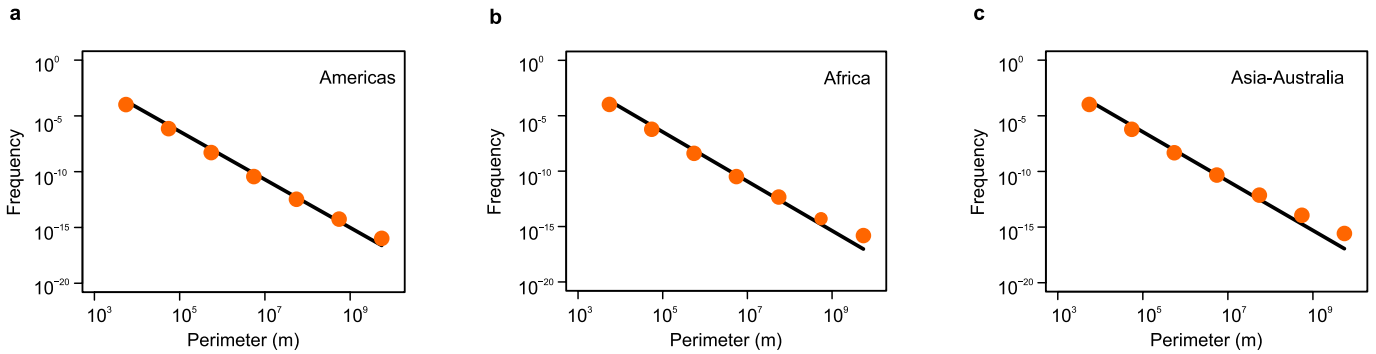

Extended Data Figure 1 | Continental-scale fragment perimeter distribution of tropical and subtropical forest. a–c, Observed fragment perimeter distributions (orange dots; fragment perimeters >1,000 m) for the Americas (**a**, $n = 55.5$ million fragments), Africa (**b**, $n = 44.8$ million fragments) and Asia–Australia (**c**, $n = 30.5$ million fragments); solid black lines show the fitted power laws with exponent κ. Forest fragments were estimated from Hansen's forest cover map[2] (see Methods for details).

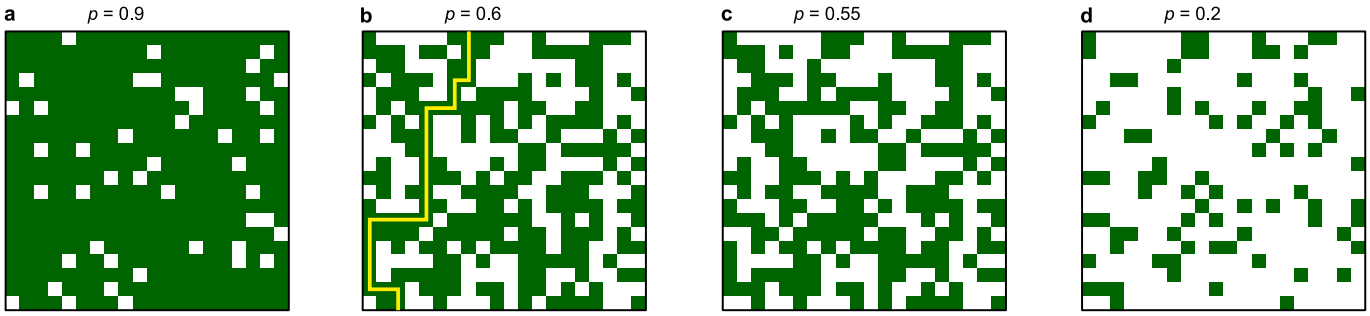

Extended Data Figure 2 | Illustration of the concept of classical percolation theory. a, A landscape occupied by 90% randomly and independently distributed forest cells (green, $p = 0.9$) is dominated by one large cluster. **b**, For values of p larger than the percolation threshold ($p = 0.6 > 0.59$) there exists a continuous path from two opposite-side borders (yellow path within the spanning cluster). **c**, Below the percolation threshold (here, $p = 0.55 < 0.59$) larger clusters emerge but no spanning cluster can be detected. **d**, A landscape occupied by 20% forest shows small unconnected clusters. Landscape size is 20×20 cells.

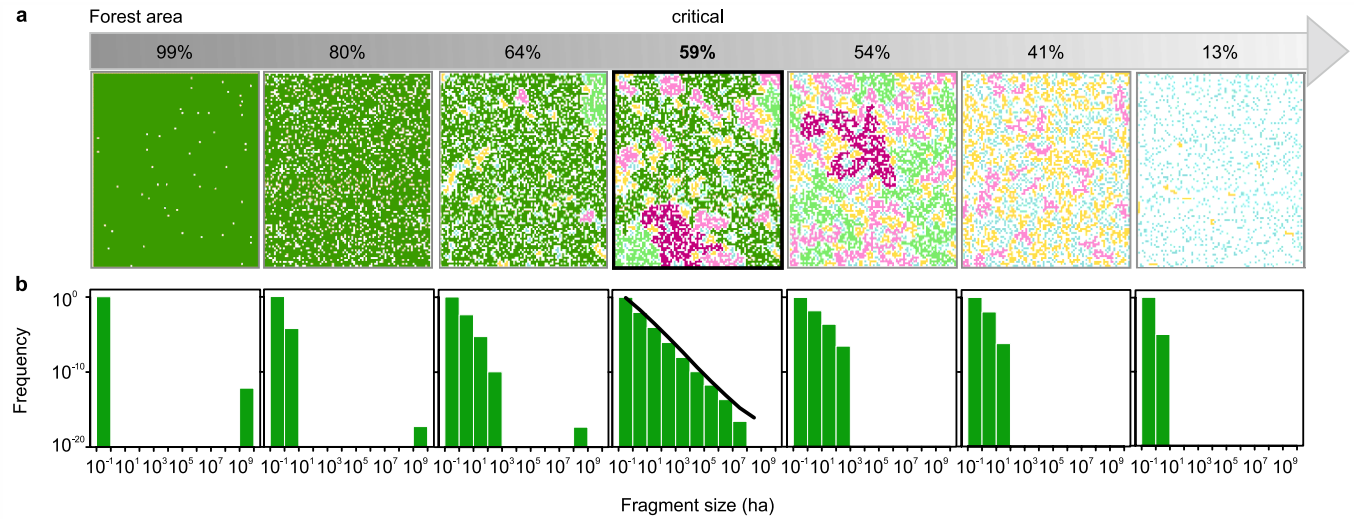

Extended Data Figure 3 | Dynamics of tropical forest fragmentation in the Americas (FRAG model). a, Spatial patterns of fragments for different snapshots in time, and **b**, fragment size distributions (green bars indicate values from the FRAG model, solid black line indicates observation from remote sensing; fragment sizes ≥ 0.1 ha). The critical phase at which the spanning fragment disappears is indicated as 'critical'. For each phase, a map of a selected subarea of 900 ha is shown (from the FRAG model, cleared sites are white and colours indicate fragment size; see Methods for details). See also Supplementary Video 1.

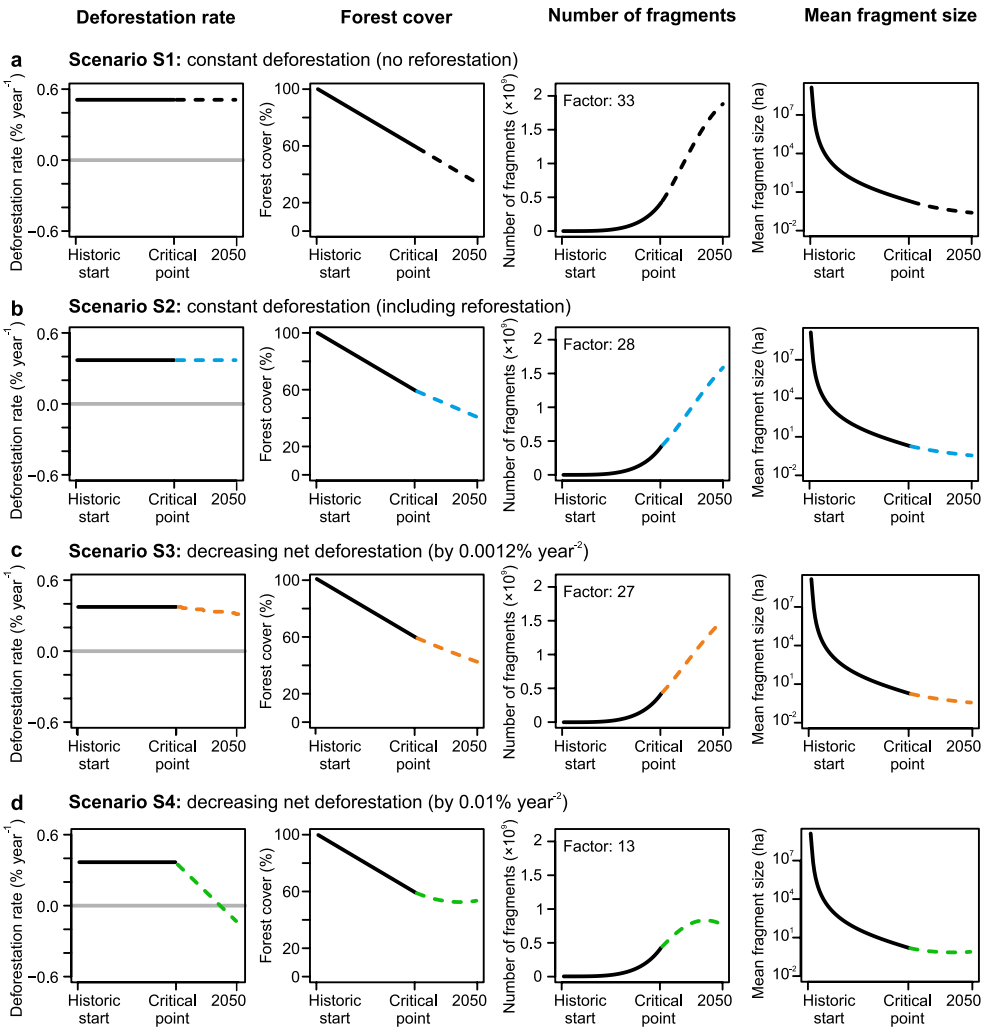

e Results of scenarios

	Observation*	Scenario S1†	Scenario S2†	Scenario S3†	Scenario S4†
Number of fragments (×10^6)	55.5	1,880.4	1,587.4	1,507.2	772.1
Mean fragment size (ha)	17	0.25	0.35	0.39	0.95

* year 2000
† for year 2050

Extended Data Figure 4 | Dynamics of fragmentation scenarios projected until 2050. Dynamics of deforestation rate (percentage per year related to landscape size), forest cover (%), number of fragments and mean fragment size (in ha) in America projected until 2050 using the FRAG model. **a**, Scenario S1 assumes constant deforestation without reforestation. **b**, Scenario S2 considers added reforestation. **c**, Scenario S3 assumes that deforestation decreases yearly. **d**, Scenario S4 considers a stronger yearly reduction in deforestation, leading to a turning point with net reforestation. See Methods for details. **e**, Comparison of observed (Table 1) and projected fragment numbers (rounded) and mean fragment size.

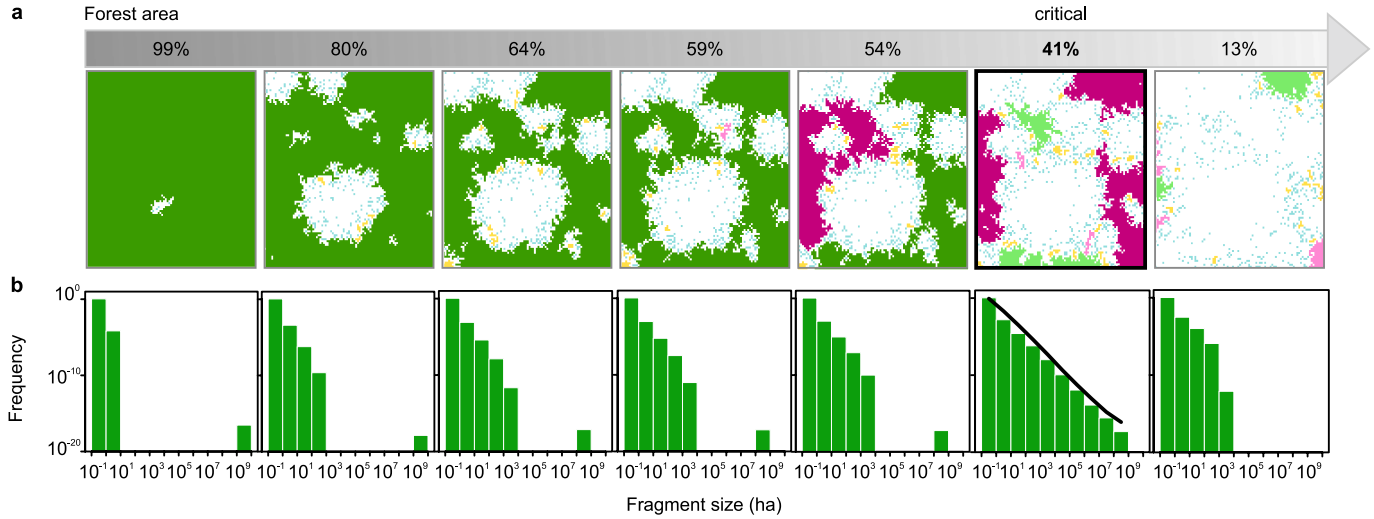

Extended Data Figure 5 | Dynamics of tropical forest fragmentation in the Americas (FRAG-B model). a, Spatial patterns of fragments for different snapshots in time, and **b**, fragment size distributions (green bars indicate values from the FRAG-B model, $d_{\mathrm{border}} = 0.995$; solid black line denotes observation from remote sensing; fragment sizes ≥ 0.1 ha). The critical phase at which the spanning fragment disappears is indicated as 'critical'. For each phase, a map of a selected subarea of 900 ha is shown (from the FRAG-B model, cleared sites are white and colours indicate fragment size; see Methods for details). See also Supplementary Video 2.

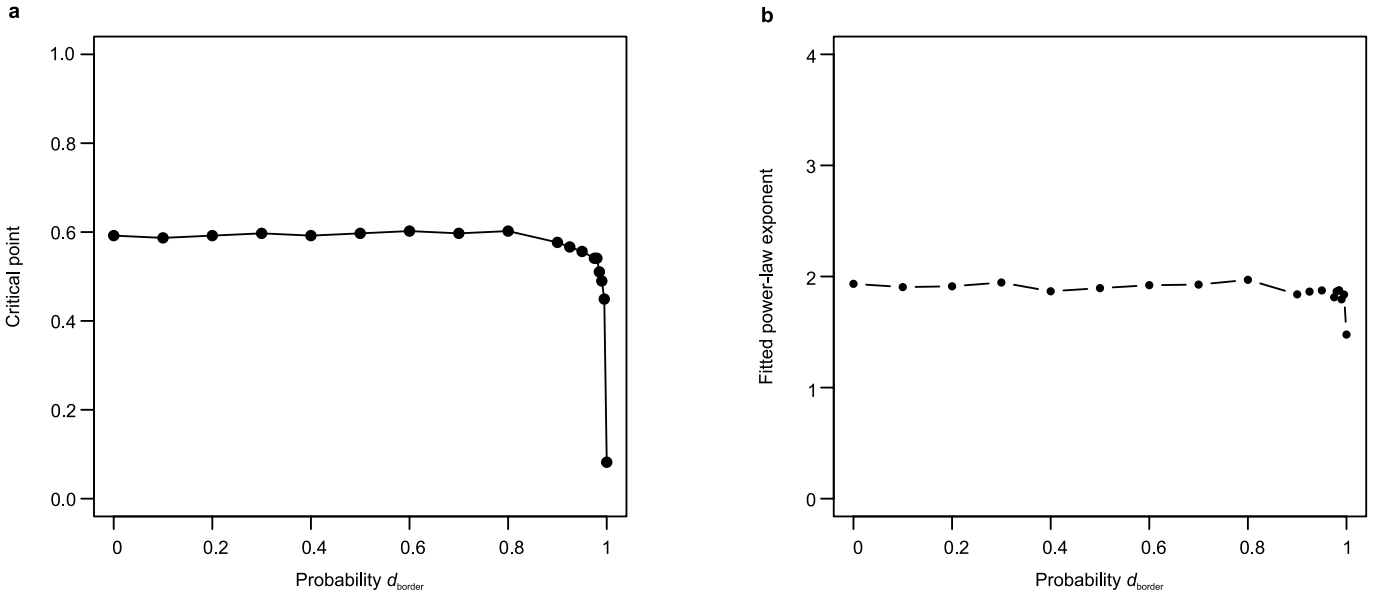

Extended Data Figure 6 | The effect of border deforestation on fragmentation dynamics. a, Critical points and **b**, fitted power-law exponents of fragment sizes for different probabilities (d_{border}) of deforestation restricted to the border of forest fragments (FRAG-B model for landscape size of $C_{max} = 10^6$ cells). Each point in **b** represents one power-law fit based on $n = 29{,}788$ ($d_{border} = 0$) to $n = 1{,}278$ ($d_{border} = 1.0$) fragments (see Methods for detailed values). Calculated R^2 values of fits are approximately 1 for the entire range of d_{border} probabilities (see Methods).

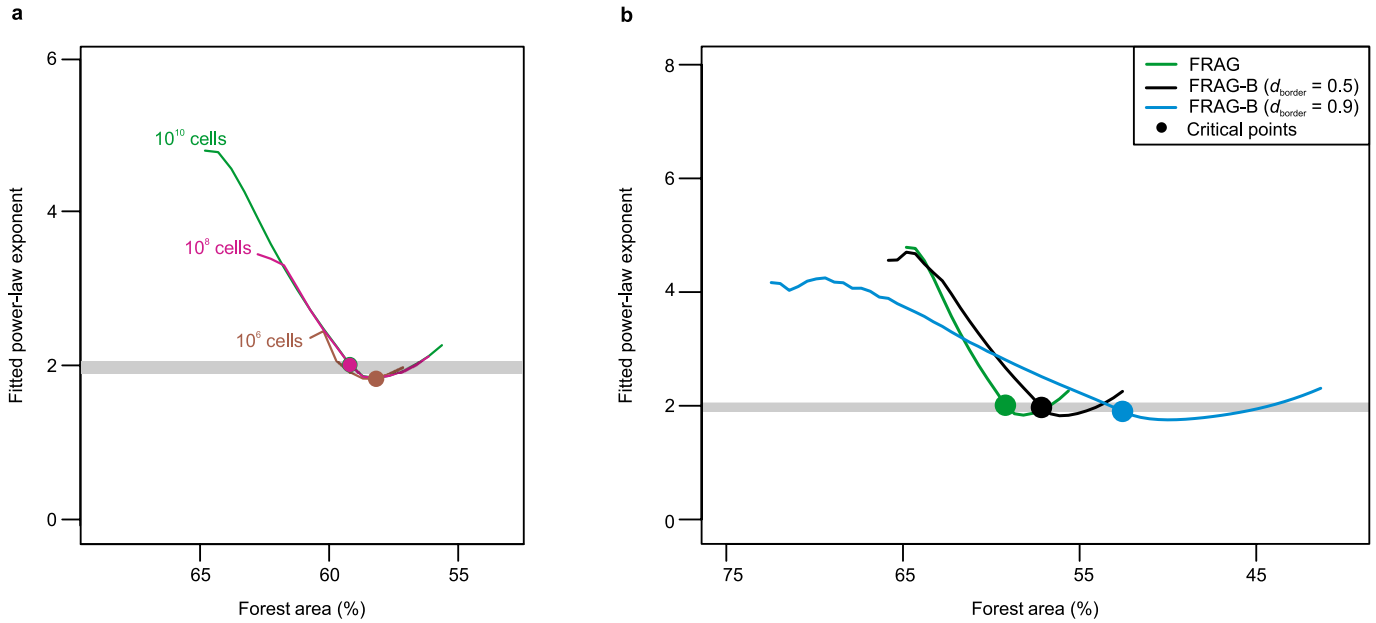

Extended Data Figure 7 | Power-law exponents fitted to simulated fragment size distributions. a, For different landscape sizes, with C_{max} based on the FRAG model. **b**, Comparison between random (FRAG model) and border deforestation (FRAG-B model, $d_{border} = 0.5$ and $d_{border} = 0.9$). In **b**, the landscape size was $C_{max} = 10^{10}$ cells. In both **a** and **b** we show only results for fits with correlation coefficients R^2 of ≥ 0.9. The grey horizontal line shows the exponent predicted by percolation theory.

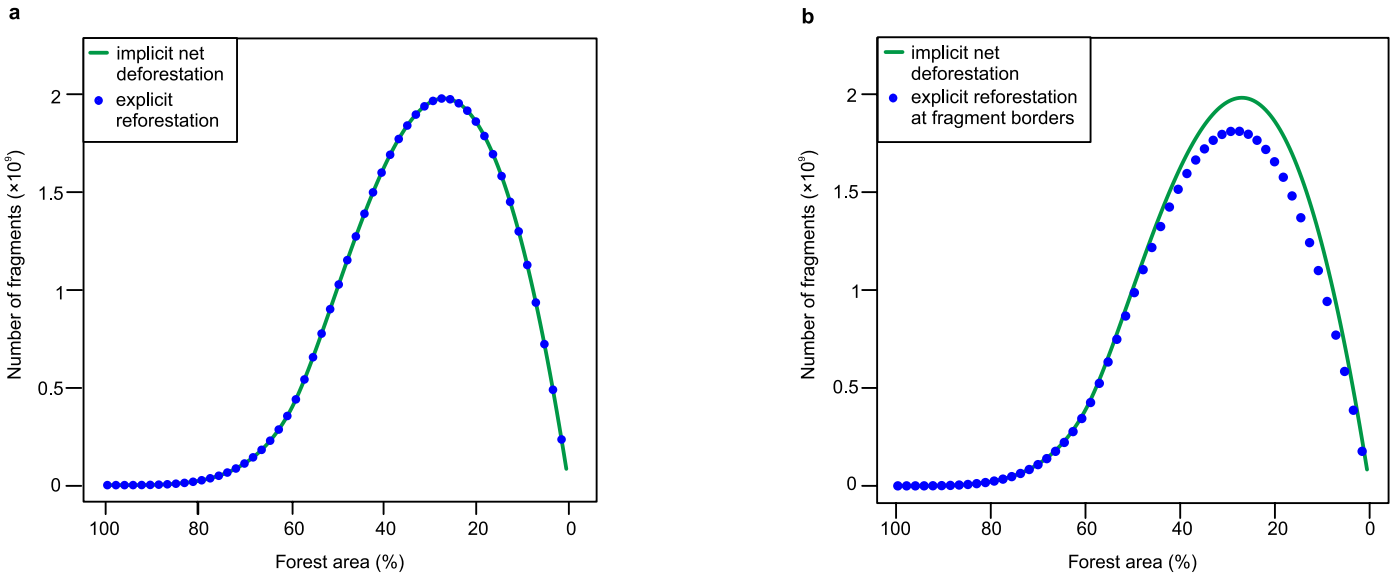

Extended Data Figure 8 | Dynamics of fragment numbers comparing implicit and explicit modelling of reforestation. a, We assume a gross deforestation rate of $d = 0.51\%$ per year and a reforestation rate of $r = 0.14\%$ per year for the Americas[1] (with random and independent selection of sites for deforestation and reforestation, blue dots). This model version is equivalent to the original FRAG model assuming a net deforestation rate of $d_{net} = 0.37\%$ per year (green line). **b**, The same scenario (green line as in **a**), but now explicit reforestation occurs exclusively at the border of forest fragments (blue dots).

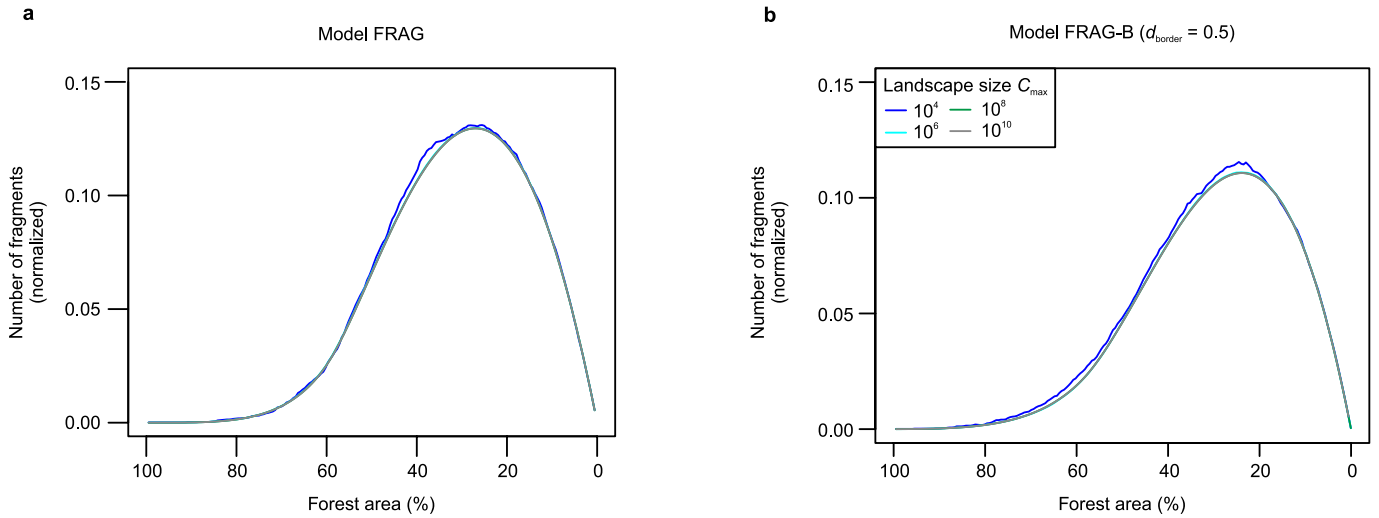

Extended Data Figure 9 | Scaling of fragmentation dynamics. Dynamics of forest fragment numbers (normalized by landscape size C_{max}) in America using **a**, the FRAG model and **b**, the FRAG-B model ($d_{border} = 0.5$) for different landscape sizes. The pattern is independent of landscape size.

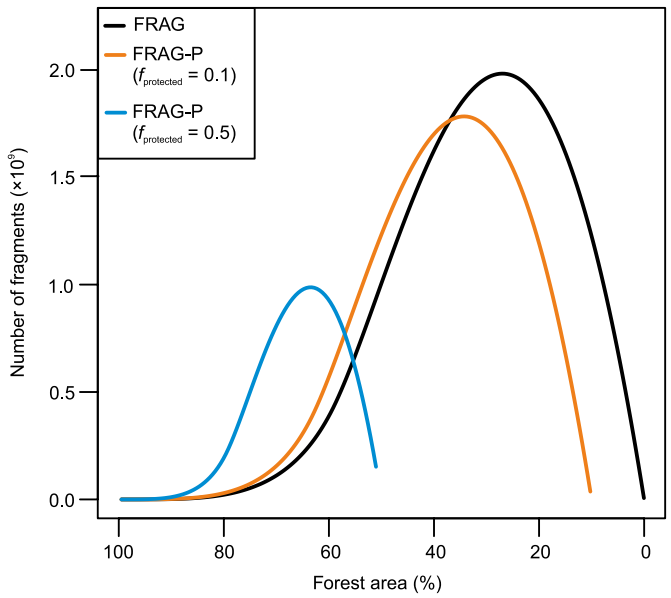

Extended Data Figure 10 | Dynamics of the number of forest fragments, without (FRAG model) and with (FRAG-P model) consideration of protected forest areas. Simulations with the FRAG-P model account for 10% ($f_{protected} = 0.1$, orange) and 50% ($f_{protected} = 0.5$, blue) of the landscape area to be protected while the remaining forest area is prone to deforestation (FRAG model). Forest areas affected by deforestation in both models were simulated using a deforestation rate of $d = 0.51\%$ per year in the Americas[1].

nature research

Corresponding author(s): Franziska Taubert

☐ Initial submission ☐ Revised version ☒ Final submission

Life Sciences Reporting Summary

Nature Research wishes to improve the reproducibility of the work that we publish. This form is intended for publication with all accepted life science papers and provides structure for consistency and transparency in reporting. Every life science submission will use this form; some list items might not apply to an individual manuscript, but all fields must be completed for clarity.

For further information on the points included in this form, see Reporting Life Sciences Research. For further information on Nature Research policies, including our data availability policy, see Authors & Referees and the Editorial Policy Checklist.

Experimental design

1. Sample size

Describe how sample size was determined.

The used global forest map has a spatial resolution of 30 m (Hansen et al. 2013 Science 342, please see Methods section "Used forest cover map and its analysis"). This is the highest spatial resolution currently available for such a product. An extended cluster detection algorithm was used to determine the forest fragments in America, Africa and Asia-Australia (please see Methods section "Used forest cover map and its analysis").

2. Data exclusions

Describe any data exclusions.

The analysis has been done for the tropics (please see Methods section "Used forest cover map and its analysis").

3. Replication

Describe whether the experimental findings were reliably reproduced.

Our study is not based on experiments, so no replication was needed. We analysed a global map on forest cover derived from remote sensing.

4. Randomization

Describe how samples/organisms/participants were allocated into experimental groups.

Our study is not based on experiments, so no randomization into experimental groups was needed.

5. Blinding

Describe whether the investigators were blinded to group allocation during data collection and/or analysis.

Our study is not based on experiments, so no group allocation and thus, no blinding was needed.

Note: all studies involving animals and/or human research participants must disclose whether blinding and randomization were used.

6. Statistical parameters

For all figures and tables that use statistical methods, confirm that the following items are present in relevant figure legends (or in the Methods section if additional space is needed).

n/a	Confirmed	
☐	☒	The exact sample size (*n*) for each experimental group/condition, given as a discrete number and unit of measurement (animals, litters, cultures, etc.)
☒	☐	A description of how samples were collected, noting whether measurements were taken from distinct samples or whether the same sample was measured repeatedly
☒	☐	A statement indicating how many times each experiment was replicated
☒	☐	The statistical test(s) used and whether they are one- or two-sided (note: only common tests should be described solely by name; more complex techniques should be described in the Methods section)
☐	☒	A description of any assumptions or corrections, such as an adjustment for multiple comparisons
☒	☐	The test results (e.g. *P* values) given as exact values whenever possible and with confidence intervals noted
☐	☒	A clear description of statistics including central tendency (e.g. median, mean) and variation (e.g. standard deviation, interquartile range)
☒	☐	Clearly defined error bars

See the web collection on statistics for biologists for further resources and guidance.

Software

Policy information about availability of computer code

7. Software

Describe the software used to analyze the data in this study.	The high-resolution forest cover map (Hansen et al. 2013 Science 342) was analysed using our developed software (available upon request, please see Methods section "Code availability"). Fragment size and perimeter distributions derived from the forest cover map were fitted to power law distributions using the Matlab package of Y. Virkar and A. Clauset (free available at http://tuvalu.santafe.edu/~aaronc/powerlaws/bins/). Simulation models of forest fragmentation (FRAG, FRAG-B and FRAG-P) were developed in C++ (available upon request, please see Methods section "Code availability"). Potential forest areas for our simulation models were calculated using climate data operators (cdo, free available at https://code.mpimet.mpg.de/projects/cdo/). Forest loss and gain data (Hansen et al. 2013 Science 342) was computed using Google Earth Engine. Basic statistical analysis were done in R (free available at https://www.r-project.org/).

For manuscripts utilizing custom algorithms or software that are central to the paper but not yet described in the published literature, software must be made available to editors and reviewers upon request. We strongly encourage code deposition in a community repository (e.g. GitHub). *Nature Methods* guidance for providing algorithms and software for publication provides further information on this topic.

Materials and reagents

Policy information about availability of materials

8. Materials availability

Indicate whether there are restrictions on availability of unique materials or if these materials are only available for distribution by a for-profit company.	Data availability statement is provided in the Methods (section "Data availability"). Data of fragment size and perimeter distributions, simulation results and the simulation models are available upon request (corresponding author). The used vegetation map can be obtained from Hansen et al. (2013) Science 342 (see references and Methods). The developed software for analysing the high-resolution forest cover map is available upon request (please see Methods section "Code availability").

9. Antibodies

Describe the antibodies used and how they were validated for use in the system under study (i.e. assay and species).	No antibodies were used in this study.

10. Eukaryotic cell lines

a. State the source of each eukaryotic cell line used.	No eukaryotic cell lines were used in this study.
b. Describe the method of cell line authentication used.	No eukaryotic cell lines were used in this study.
c. Report whether the cell lines were tested for mycoplasma contamination.	No eukaryotic cell lines were used in this study.
d. If any of the cell lines used are listed in the database of commonly misidentified cell lines maintained by ICLAC, provide a scientific rationale for their use.	No eukaryotic cell lines were used in this study.

Animals and human research participants

Policy information about studies involving animals; when reporting animal research, follow the ARRIVE guidelines

11. Description of research animals

Provide details on animals and/or animal-derived materials used in the study.	No animals were used in this study.

Policy information about studies involving human research participants

12. Description of human research participants

Describe the covariate-relevant population characteristics of the human research participants.	No human research participants were in this study.